Science Advances
AAAS

advances.sciencemag.org/cgi/content/full/4/11/eaau3487/DC1

Supplementary Materials for

Multidimensional risk in a nonstationary climate: Joint probability of increasingly severe warm and dry conditions

Ali Sarhadi*, María Concepción Ausín, Michael P. Wiper, Danielle Touma, Noah S. Diffenbaugh

*Corresponding author. Email: asarhadi@stanford.edu

Published 28 November 2018, *Sci. Adv.* **4**, eaau3487 (2018)
DOI: 10.1126/sciadv.aau3487

This PDF file includes:

SUPPLEMENTARY INFORMATION

Section S1. Datasets

1.1. Observations

We calculate the probability of warm and dry years using temperature and precipitation anomalies from the Global Historical Climatology Network (GHCN) (https://www.ncdc.noaa.gov/temp-and-precip/ghcn-gridded-products/). The GHCN dataset consists of monthly temperature anomalies, in which the value in each month of the time series is calculated as a departure from the long-term mean monthly climatology during a specified baseline period. The GHCN dataset uses 1981-2010 as the baseline period for temperature, and 1961-1990 as the baseline period for precipitation. Because we analyze the co-occurrence of years that are both warm and dry, it is important for the temperature and precipitation values to be expressed as anomalies from a uniform baseline period. To that end, we use a simple arithmetic adjustment to express each of the temperature values as an anomaly from the 1961-1990 period (i.e., adding the difference between the 1981-2010 calendar-month mean temperature and the 1961-1990 calendar-month mean temperature to each monthly temperature value at each grid point).

We calculate the annual anomaly time series of temperature and precipitation by aggregating the respective monthly anomaly time series. We sub-select those grid cells that have complete records from 1931 through 2015 for temperature and precipitation, respectively. To calculate the joint probability of warm and dry years, we only consider those grid cells that have data for both temperature and precipitation for the full 1931-2015 period.

1.2. Climate models

To study the influence of anthropogenic forcing on the concurrent risk of warm and dry years, we use global climate model simulations from Phase 5 of the Coupled Model Intercomparison Project (CMIP5) (*30*). To facilitate the comparison between climate models, we follow many previous studies and grid all climate model realizations to a common 1˚x1˚ geographical grid. When quantifying the joint probability of warm and dry years occurring simultaneously in different regions, we use all of the 1˚x1˚ grid points in each region.

1.2.1. Influence of historical anthropogenic forcing

To quantify the influence of anthropogenic forcing during the historical period, we compare the CMIP5 Historical simulations (which prescribe anthropogenic and natural climate forcings) with the CMIP5 Natural simulations (which prescribe only natural climate forcings). Both the Historical and Natural simulations are run through 2005 in the CMIP5 protocol.

We calculate the probability of warm years using the realizations that archived the surface air temperature, and the probability of dry years using the realizations that archived precipitation. The lists of realizations that archived temperature for the Historical and Natural experiments are given in column 1 and column 2 in table S1, respectively. Likewise, the lists of realizations that archived precipitation for the Historical and Natural experiments are given in column 1 and column 2 in table S2, respectively. In addition, to calculate the joint probability of warm and dry years, we analyze the available Historical realizations for which temperature and precipitation data are both archived, and the available Natural realizations for which temperature and precipitation data are both archived. The

lists of the selected realizations for the Historical and Natural experiments are given in column 1 and column 2 in table S3, respectively.

For the regional analysis (see Section 2.2), we test the statistical significance of the difference in the underlying probabilities between the CMIP5 Historical and Natural experiments using the Kolmogorov-Smirnov test. We first calculate the joint probabilities for each region pair during the 1931-1950, 1961-1980 and 1986-2005 periods of the Historical and the Natural simulations, respectively. Then, for each region pair in each of the three time periods, we use the bootstrap Kolmogorov-Smirnov test to compare the population of joint probabilities in the Historical simulations with the population of joint probabilities in the Natural simulations (at the 1% and 5% significance levels). For quantifying the statistical significance of differences in the joint probability of warm years in each region pair, we use each realization that archived temperature (see column1 and column 2 in table S1). Similarly, for quantifying the statistical significance of differences in the joint probability of dry years in each region pair, we use each realization that archived precipitation (see column 1 and column2 in table S2). Further, for quantifying the statistical significance of differences in the joint probability of warm+dry years in each region pair, we analyze each realization that archived both temperature and precipitation (see column 1 and column 2 in table S3 for the list of the Historical and Natural realizations).

1.2.2. Comparisons of future anthropogenic forcing

In order to quantify the impact of elevated climate forcing on the concurrent risk of warm and dry years in each region pair, we also compare the joint probability of warm, dry, and warm+dry years in the 2020-2050 period of the RCP2.6 and RCP8.5 Representative Concentration Pathway (RCP) future climate forcing scenarios. Of the simulations archived in CMIP5, RCP8.5 is the RCP that most closely tracks the recent emissions trajectory, while RCP2.6 is the RCP that most closely represents the ambitious mitigation detailed in the United Nations Paris Agreement (*31*). The global warming in the mid-century of RCP8.5 is approximately 2-3˚C above the pre-industrial (similar to the Nationally Determined Contributions agreed upon in the UN Paris Agreement), while the global warming in the mid-century of RCP2.6 is approximately 1-2˚C above the pre-industrial (similar to the aspirational goals agreed upon in the UN Paris Agreement). Therefore, comparing the joint probability of warm, dry, and simultaneously warm and dry years for the 2020-2050 period of RCP8.5 and RCP2.6 allows us to quantify the difference in the risk of concurrent climate stresses for forcing levels consistent with the UN targets and commitments.

We combine the Historical (1931-2005) and RCP (2006-2050) periods in each realization to generate continuous time series (1931-2050) of temperature and precipitation. We therefore select realizations for each future scenario that have a corresponding archived Historical realization. For example, to quantify the future probability of co-occurring warm years in each region pair in RCP2.6, we select the realizations that archived temperature in both the Historical and RCP2.6 experiments (see column 3 in table S1). Likewise, to quantify the future probability of co-occurring dry years in each region pair in RCP2.6, we select the realizations that archived precipitation in both the Historical and RCP2.6 experiments (see column 3 in table S2). Further, to quantify future probability of co-

occurring warm+dry years in each region pair in RCP2.6, we select the realizations that archived both temperature and precipitation in both the Historical and RCP2.6 experiments (see column 3 in table S3).

Section S2. Methodology

Anthropogenic global warming is changing the nature of the water cycle and hydro-climatic processes (*2*). These changes exacerbate the risk of extreme climate phenomena through time. However, most of the analytical risk approaches currently in use assume that the probabilistic characteristics of extreme hydro-climatic events will not change through time. This assumption is against the dynamic (non-stationary) conditions arising from climate change, which change the probabilistic behavior of extreme events (*9*, *10*). Therefore, to account for changes in the climate system, stationarity-based risk methods should be updated to allow for flexible, time-varying risk quantification. In this new approach, statistical distribution functions are expressed as a function of covariates in order to model non-stationary conditions arising from global warming. The present study introduces a new dynamic, Bayesian framework for univariate and multivariate non-stationary risk analyses. The framework is applied to calculate the temporal and spatial time-varying probability of warm years, dry years, and the joint condition of warm and dry years occurring in an individual location and simultaneously in multiple locations.

2.1 Temporal probability of warm and dry years

2.1.1.Time-varying marginal distributions

2.1.1.1 Distribution and trend model selection

Assume that $T_{(t)}$ and $P_{(t)}$ represent annual temperature and precipitation anomalies, starting at real time *t*. Under non-stationary conditions arising from climate change, it may happen that the behavior of the anomalies changes over time, and their probabilistic parameters may no longer be constant. In this condition, using stationary-based models, which assume static parameters for the moments of the time series, may lead to high uncertainty in the risk assessment outputs (*14*, *25*). An alternative approach should thus be developed, so that the effect of non-stationarity is integrated and the probabilistic parameters are allowed to change over time. For example, assume that the mean of each time series is detected to change over time under non-stationary conditions. Accordingly, a time-varying distribution should be designed to express the changes in the mean of the time series through time. In addition to the type of distribution function, the form of trend model (linear or nonlinear) should also be selected to express the time-varying moment in each anomaly under non-stationary conditions.

In the current study, we develop a non-stationary risk framework that accounts for changes in the mean of multiple climate variables as a function of time (as the covariate). The steps of this non-stationary algorithm for marginal anomalies are illustrated in a schematic flowchart in fig. S1. Firstly, it is necessary to select which form of linear and nonlinear trend can represent time-dependent changes in the mean (location parameter) of the anomalies. To do so, classical polynomial regression models using orthogonal polynomials with normal errors are fitted to the anomalies. In general, we can model the expected value of the location parameter as a k^{th} degree polynomial through

time, capturing any type of linear or nonlinear trend in the mean. Here, in order to prevent over fitting, we only consider polynomial regression models up to the fourth degree to detect trends in the location parameter. Also, because direct polynomial models can be associated with problems of multicolinearity in their fitting, we apply orthogonal polynomials to avoid these difficulties.

Different degrees of the orthogonal polynomial regression models, consisting of constant, linear, quadratic, and the third degree polynomial models in terms of location parameter for temperature anomalies, are given as follows

$$\mu_{T_{(t)}}^{k} = \eta_0 + \sum_{i=1}^{k} \eta_i p_i(t) + \varepsilon_\eta(t) \quad (1)$$

where $p_i(t)$ is a polynomial of order i such that $p_i(t)p_j(t) = 0$ for all $j \neq i$. t is time, η_{0-3} are polynomial regression coefficients regarding the k^{th} order of time-varying location parameter ($\mu_{T_{(t)}}^{k}$) for temperature anomalies, and $\varepsilon_\eta(t)$ is an unobserved random error (residual) with zero mean and unit variance. The same polynomial regression models can be used to estimate the k^{th} order of time-varying location parameter ($\mu_{P_{(t)}}^{k}$) for precipitation anomalies, given by

$$\mu_{P_{(t)}}^{k} = \theta_0 + \sum_{i=1}^{k} \theta_i p_i(t) + \varepsilon_\theta(t) \quad (2)$$

where θ_{0-3} denote polynomial regression coefficients for time-dependent location parameter, and $\varepsilon_\theta(t)$ is an unobserved random error (residual) with zero mean and unit variance for precipitation. The rest of the parameters are similar to the ones given in equation 1.

The Akaike Information Criterion (AIC) is used to select the optimal fitted regression model. By refitting the best-selected polynomial regression model, the residual of the model can then be calculated. In polynomial regression models (or generally in regression analysis), the variances of the residuals may differ from one data point to another, even if the variances of the errors are equal in each data point. Therefore, prior to fitting normal distribution to the time series, we studentize the residuals to make sure that they are normalized to unit variance. The Kolmogorov-Smirnov (K-S) test is then applied to evaluate whether the residuals are normally distributed. If the K-S test is passed, that means the residuals are normally distributed and we conclude that the time-varying normal distribution can model changes in the mean of the anomalies.

Upon selection of the distribution, the time-varying normal distribution can be written as follows for both temperature and precipitation anomalies

$$\begin{aligned} T_{(t)} | \, \mu_{T_{(t)}}, \sigma &\sim N\left(\mu_{T_{(t)}}, \sigma^2\right) \\ P_{(t)} | \, \mu_{P_{(t)}}, \gamma &\sim N\left(\mu_{P_{(t)}}, \gamma^2\right) \end{aligned} \quad (3)$$

with probability distribution functions given as

$$f\left(T_{(t)}\middle|\mu_{T_{(t)}},\sigma^2\right)=\frac{1}{\sqrt{2\pi\sigma^2}}e^{-\frac{(T_t-\mu_{T_{(t)}})^2}{2\sigma^2}}$$
$$f\left(P_{(t)}\middle|\mu_{P_{(t)}},\gamma^2\right)=\frac{1}{\sqrt{2\pi\gamma^2}}e^{-\frac{(P_{(t)}-\mu_{P_{(t)}})^2}{2\gamma^2}} \quad (4)$$

where $\mu_{T_{(t)}}$ and $\mu_{P_{(t)}}$ are the time-dependent location parameters, modeled by the already selected polynomial normal-tail regression models in equation 1 and equation 2, representing the best-fitted linear or nonlinear trends in the mean of temperature and precipitation anomalies as a function of time, respectively. σ and γ are also scale parameters of the normal distributions.

Therefore, if the normal distribution is passed from the K-S test, and for example a quadratic regression model selected to represent trends in the time series, a set of model parameters is given by $\beta_{1_T}=(\eta_0,\eta_1,\eta_2,\sigma)$ for temperature anomalies, and also $\beta_{1_P}=(\theta_0,\theta_1,\theta_2,\gamma)$ for precipitation anomalies, to define a time-varying normal distribution.

In contrast, if the K-S test is rejected, that means the residuals are not well-fitted to the normal distribution, and a heavy-tailed distribution should be replaced to better model outlying values in the anomalies. One of the optimum distributions is Student's *t* distribution, which is a symmetric and heavy-tailed distribution as a special case of generalized hyperbolic distribution (*33*). In the next step in the algorithm, after calculating optimal degree of freedom, the classical orthogonal regression models are re-fitted, considering heavy tail (Student's *t*) distributed errors. The Student's *t* distribution is much more flexible in fitting to heavy tailed data than the normal regression model. Although in the case of the Student's *t* regression model, no standard goodness of fit test is available, the residual distributions in all cases of the climate variable time series for NOAA observations are symmetric, indicating a good fit of this model.

The heavy tail error regression models for temperature anomalies are given as follows

$$\mu_{T_{(t)}}^{k}=\delta_0+\sum_{i=1}^{k}\delta_i p_i(t)+\varepsilon_\delta(t) \quad (5)$$

where δ_{0-3} are heavy tail error regression coefficients for temperature anomalies, and $\mu_{T_{(t)}}^{k}$ is the k^{th} order of time-varying location parameter, capturing any types of non-stationarity in the time series. $\varepsilon_\delta(t)$ is an unobserved random error (residual) with zero mean and unit variance for temperature time series.

The same heavy tail error regression models can also be formulated for precipitation anomalies, given by

$$\mu_{P_{(t)}}^{k}=\phi_0+\sum_{i=1}^{k}\phi_i p_i(t)+\varepsilon_\phi(t) \quad (6)$$

where $\mu_{P_{(t)}}^{k}$ is the k^{th} order of time-varying location parameter, defined by different forms of heavy tail multiple regression models (with different combination of the coefficients ϕ_{0-3}). $\varepsilon_\phi(t)$ is also a random error (residual) with zero mean and unit variance for precipitation time series.

Selecting the best-fitted polynomial regression models (using AIC), the time-dependent location parameters in the anomalies are modeled using time-varying Student's *t* distributions. The developed time-varying Student's *t* distribution for the anomalies is thus given as follows

$$\begin{aligned} T_{(t)} | \, \mu_{T_{(t)}}, \rho \; &\sim t \; \left(\nu_T, \mu_{T_{(t)}}, \rho^2\right) \\ P_{(t)} | \, \mu_{P_t}, \kappa \; &\sim t \; \left(\nu_P, \mu_{P_{(t)}}, \kappa^2\right) \end{aligned} \tag{7}$$

where $\mu_{T_{(t)}}$and $\mu_{P_{(t)}}$ are the time-varying location parameters, modeled based on the best polynomial heavy tail regression models. ρ and κ are also scale parameters of the time-varying Student's *t* distributions.

The probability density functions of the time-varying Student's *t* distributions in the non-stationary conditions is thus given as follows

$$f\left(T_{(t)}\right) = \frac{\Gamma(\frac{\nu_T + 1}{2})}{\rho\sqrt{\nu_T \pi}\Gamma(\frac{\nu_T}{2})}\left[\frac{\nu_T + (\frac{T_{(t)} - \mu_{T_{(t)}}}{\rho})^2}{\nu_T}\right]^{-(\frac{\nu_T+1}{2})}$$

$$f\left(P_{(t)}\right) = \frac{\Gamma(\frac{\nu_P + 1}{2})}{\kappa\sqrt{\nu_P \pi}\Gamma(\frac{\nu_P}{2})}\left[\frac{\nu_P + (\frac{P_{(t)} - \mu_{P_{(t)}}}{\kappa})^2}{\nu_P}\right]^{-(\frac{\nu_P+1}{2})} \tag{8}$$

where ν_T and ν_P are the degrees of freedom in each distribution, and they are calculated for each marginal Student's *t* distribution, separately.

Similar to the time-varying normal distributions, based on the best selected trend model in the time-dependent location parameters (for instance a quadratic model), a set of parameters is given by $\beta_{2_T} = (\delta_0, \delta_1, \delta_2, \rho)$ and $\beta_{2_P} = (\phi_0, \phi_1, \phi_2, \kappa)$ to define a time-varying Student's *t* distribution, for temperature and precipitation anomalies, respectively.

In principle, the developed methodology in this study allows us to model changes in the mean of temperature and precipitation anomaly time series through time. If there are any time-trend changes in the relevant variance terms, it will be possible to extend the methodology to model changes in variability, by assuming that the scale parameter ($\log \sigma^2$) is a function of time as well. In this study, however, after modeling the time-trend changes in the mean of the climate variables using normal and Student's *t* distributions, there is no evidence of any trend in the residuals of the models (fig. S3). To test this, after fitting the time-trend polynomial regression models on the mean of temperature and precipitation anomaly time series of the NOAA observations (1931-2015), a Block Bootstrapping Mann-Kendall trend analysis is applied on the residuals of the models in each grid point. Figure S3 shows the results of p-values given by the trend analysis on the residuals of the climate variables. The p-values in all the locations are greater than 0.05, which indicates that the null hypothesis of no trend in the residuals cannot be rejected.

2.1.1.2 Bayesian inference and marginal distributions

Characterizing uncertainty in a time-varying non-stationary risk framework is of crucial importance to enhance the reliability of the risk assessment. To quantify uncertainty of the time-varying distributions, a Bayesian Markov Chain Monte Carlo (MCMC) approach is used to estimate the parameters of the marginal temperature and precipitation distributions.

Bayesian inference defines prior distributions for all unknown polynomial regression model parameters (upon detection of the trend in the location parameter). Given the observed data, the prior distributions are then updated into posterior distributions, which combine prior knowledge and data via Bayes' Theorem.

Suppose that we have a sample of temperature anomalies, $T_{t_1}, \dots, T_{t_n}$ for time steps $t_1, \dots, t_n$. Assume that a time-varying normal distribution with a quadratic trend in the location parameter is fitted to the time series. The posterior distribution for the time-varying distribution parameters, $\beta_T = (\eta_0, \eta_1, \eta_2, \sigma)$ can then be formulated as follows:

$$p\left(\beta_T \middle| T_{t_{(1)}}, \dots, T_{t_{(n)}}\right) \propto p(\beta_T) \prod_{\mathrm{i}=1}^{\mathrm{n}} p\left(T_{t_{(i)}} \middle| \beta_T\right) \tag{9}$$

where $p(\beta_T)$ is the prior distribution and the densities in the likelihood function are given by

$$p\left(T_{t_{(i)}} \middle| \beta_T\right) = \frac{1}{\sqrt{2\pi\sigma^2}} \mathrm{e}^{-\frac{\left(T_{(t)} - \mu_{T_{(t)}}\right)^2}{2\sigma^2}} \tag{10}$$

where the time varying mean is $\mu_{T_{(t)}} = \eta_0 + \eta_1 t + \eta_2 t^2$. The updated posterior distribution, $p\left(\beta_T \middle| T_{t_{(1)}}, \dots, T_{t_{(n)}}\right)$, thus provides information on the posterior distribution of the time-varying location parameter, $\mu_{T_{(t)}}$ for each time step *t*. In the case of the stationary condition, it should be noted that the location parameter remains constant ($\mu_{T_{(t)}} = \eta_0$), and temperature anomalies will be independent and identically distributed (*iid*). Regarding the prior distributions $p(\beta_T)$, they provide prior knowledge on the set of parameters, β_T, from external source of information, independently from observations. In the given example, prior information is assumed as, $\eta_{0-2} \sim N\ (0, 1000)$, and $\sigma \sim U\ (0, 100)$.

The same, above-mentioned process can be followed for Student's *t* distribution, as well as the time-varying distributions fitted to precipitation anomalies with different types of trend in the mean.

To estimate the Bayesian posterior parameter distribution, an MCMC sampling approach is used to generate an approximate sample of realizations from the posterior. Although there are different types of algorithms for MCMC sampling, in this study, we use the Gibbs sampling approach. The Gibbs sampler algorithm utilizes a specified multi-dimensional probability density function to obtain a sequence of observations, by having all the parameters fixed except one (*13*, *34*). In other words, the algorithm yields sequences on each parameter through iterative sampling from the full conditional distributions. To assess the convergence of the Markov chain, a convergence diagnosis test introduced by Gelman and Rubin [1992] (*35*) is used. According to the test, the convergence is

achieved if the Gelman and Rubin (GR) index is less than 1.2. In the all cases for the marginal distributions, GR index is set to 1.0 for all parameters in different forms of trends after 10,000 iterations in one chain, with 3000 iterations used for burn-in.

After estimating time-dependent location parameters using the MCMC Bayesian inference framework, the time-varying probabilities related to warm years and dry years can be calculated from the temperature and precipitation anomalies depending on which distribution has been fitted. If a normal distribution is fitted to the anomalies, the time-varying warm and dry year probabilities are then calculated using the time-varying normal distributions as follows

$$\Pr(T_{t_{(1)}} > 0, \dots, T_{t_{(n)}} > 0 \mid \{\mu_{T_{(t)}}, \sigma\}_{t=t_{(1)}}^{t_{(n)}}) = \prod_{t=t_{(1)}}^{t_{(n)}} (1 - F_{T_{(t)}}(T_t = 0 | \mu_{T_{(t)}}, \sigma))$$

$$\Pr(P_{t_{(1)}} < 0, \dots, P_{t_{(n)}} < 0 \mid \{\mu_{P_{(t)}}, \gamma\}_{t=t_{(1)}}^{t_{(n)}} = \prod_{t=t_{(1)}}^{t_{(n)}} (F_{T_{(t)}}(P_t = 0 | \mu_{P_{(t)}}, \gamma)) \quad (11)$$

where $\Pr(T_{t_{(1)}} > 0, \dots, T_{t_{(n)}} > 0)$ and $\Pr\left(P_{t_{(1)}} < 0, \dots, P_{t_{(n)}} < 0\right)$ are the conditional, time-varying probability of warm years and dry years, respectively.

In contrast, if Student's *t* distribution is fitted to the anomalies, then the same process is followed using the time-varying Student's *t* distributions, and the time-dependent warm year and dry year probabilities are given by:

$$\Pr(T_{t_{(1)}} > 0, \dots, T_{t_{(n)}} > 0 \mid \{\mu_{T_{(t)}}, \rho, \nu_T\}_{t=t_{(1)}}^{t_{(n)}}) = \prod_{t=t_{(1)}}^{t_{(n)}} (1 - F_{T_{(t)}}(T_t = 0 | \mu_{T_{(t)}}, \rho, \nu_T))$$

$$\Pr(P_{t_{(1)}} < 0, \dots, P_{t_{(n)}} < 0 \mid \{\mu_{P_{(t)}}, \kappa, \nu_P\}_{t=t_{(1)}}^{t_{(n)}}) = \prod_{t=t_{(1)}}^{t_{(n)}} (F_{T_{(t)}}(P_t = 0 | \mu_{P_{(t)}}, \kappa, \nu_P)) \quad (12)$$

It should be noted that the uncertainty and the Bayesian credible intervals of the time-varying probabilities can be estimated based on different quantiles of sampling in the posterior distributions. In this study, to better provide information about the precision of the time-varying probabilities, Bayesian credible intervals are estimated using the 2.5% and 97.5% percentiles of the MCMC sampled values.

2.1.2 Joint distribution using Bayesian time-varying copulas

To calculate the temporal joint probability of warm year and dry year occurrences, we use copulas as flexible tools for constructing multivariate distributions and modeling the dependence structure between warm and dry conditions. Copulas are popular due to their flexibility in modeling the dependence structure between multiple attributes using any types of marginal distribution (*36*). Upon the detection of any trends in the marginals, a time-dependent copula can be developed to characterize the relationship of the time-varying marginals in a more flexible and dynamic manner under non-stationary conditions. Suppose that $y_t = (y_{1t}, y_{2t})$ represents a pair of time-dependent climate

variables. A general time-varying copula can be developed to model the dependence structure between time-varying variables given by

$$F\left(y_{(t)}\middle|\theta_c\right) = C\left(F_1\left(y_{1_{(t)}}\middle|\theta_{1_{(t)}}\right), F_2\left(y_{2_{(t)}}\middle|\theta_{2_{(t)}}\right)\middle|\theta_c\right) \qquad F\left(y_{(t)}\middle|\theta_c\right) = C\left(u_{1_{(t)}}, u_{2_{(t)}}\middle|\theta_c\right) \tag{13}$$

where $F(.)$ denotes cumulative distribution function, $C(.)$ is the copula function, $\theta_{1_{(t)}}$ and $\theta_{2_{(t)}}$ are the set of parameters of the time-varying marginal models, θ_c is the copula parameter, and $u_{1_{(t)}}$ and $u_{2_{(t)}}$ are the time-varying marginal probabilities in the unit hypercube with uniform marginal distributions $U[0,1]$.

To extend a Bayesian version of equation 13 for the copula analysis and calculate time-dependent joint probability of warm and dry years, assume that the marginals (temperature and precipitation anomalies) are fitted to two different time-varying normal and Student's *t* distributions, respectively. The mean (location parameter) in each of these marginal distributions also follows a quadratic trend model in a non-stationary condition. The posterior distribution for the joint condition based on Bayes' Theorem is then given by

$$\mathrm{p}\left(\boldsymbol{\Theta}\middle|\{T_{(t)}, P_{(t)}\}_{t=1}^{n}\right) \propto \mathrm{p}(\boldsymbol{\Theta}) \prod\nolimits_{t=1}^{n} f(T_{(t)}, P_{(t)} \mid \boldsymbol{\Theta}) \tag{14}$$

where $f(T_{(t)}, P_{(t)} \mid \boldsymbol{\Theta})$ is the joint density function of temperature and precipitation anomalies, which can be written in terms of a copula function as follows

$$f(T_{(t)}, P_{(t)} \mid \boldsymbol{\Theta}) = c\left(F_1\left(T_{(t)}\middle|\{\mu_{T_{(t)}}, \sigma\}\right), F_2\left(P_{(t)}\middle|\left\{\mu_{P_{(t)}}, \gamma\right\}\right)\middle|\theta_c\right) \times f_1\left(T_{(t)}\middle|\{\mu_{T_{(t)}}, \sigma\}\right) f_2\left(P_{(t)}\middle|\{\mu_{P_{(t)}}, \gamma\}\right)$$

$$\mu_{T_{(t)}} = \eta_0 + \sum_{i=1}^{2} \eta_i p_i(t) + \varepsilon_\eta(t)$$

$$\mu_{P_{(t)}} = \phi_0 + \sum_{i=1}^{2} \phi_i p_i(t) + \varepsilon_\phi(t) \tag{15}$$

where *c* is the copula density function depending on the parameter(s), θ_c , and f_1 and f_2 are the marginal density functions, respectively for the temperature and precipitation anomalies given in equation 4 for the Gaussian case or equation 8 for the Student's *t* case. Then, the joint posterior of the parameter set $\boldsymbol{\Theta} = [\eta_{0-2}, \phi_{0-2}, \sigma, \kappa, \theta_c]$ can be formulated in the following equation after substituting prior distributions in equation 14

$$\mathrm{p}(\boldsymbol{\Theta}|\{T_{(t)}, P_{(t)}\}_{t=1}^{n}) = \prod_{t=1}^{n} f(T_{(t)}, P_{(t)} \mid \boldsymbol{\Theta}) \times \prod_{i=0}^{2} N\left(\eta_{(i)}\middle|0, 10^3\right) \times N\left(\phi_{(i)}\middle|0, 10^3\right) \times U(\sigma|0, 10^2) \times U(\kappa|0, 10^2) \times U(\theta_c \mid \theta_{min}, \theta_{max}) \tag{16}$$

Here, θ_c is the copula parameter(s), which describe(s) the dependence structure between the time-varying probability of the marginals (warm and dry-years). For this parameter, we assume a uniform prior defined between two values ($\theta_{min}, \theta_{max}$), which depend on the copula model. In this study, different types of copulas (including Elliptical and Archimedean copula families) are used to represent different forms of dependency between the time-dependent marginals. The bivariate copula functions used in the present study include Gaussian, Student's *t* (*t*-

copula), Clayton, Frank, Gumbel, and Joe copulas. The mathematical descriptions of the underlying copulas are given in table S4. More information about the functions of these copulas can be found in *Sadegh et al.* (*23*). In terms of the goodness-of-fit test, Deviance Information Criterion (DIC) is used to select the best-fitted copula for each pair of marginal.

Defining an MCMC algorithm to sample from the joint posterior distribution (equation 16) is very time consuming. Therefore, as is usually done in copula settings, we employ a two-step approach where we firstly estimate the marginal parameters, $(\eta_{0-2}, \phi_{0-2}, \sigma, \kappa)$, using the Bayesian approach described in section 2.1.1.2. Given the marginal estimations, we obtain the copula data, $\{u_{(t)}, v_{(t)}\}_{t=1}^{n}$, based on the posterior means of $u_{(t)}=F_1\left(T_{(t)}\middle|\{\mu_{T_{(t)}}, \sigma\}\right)$ and $v_{(t)} = F_2\left(P_{(t)}\middle|\{\mu_{P_{(t)}}, \kappa\}\right)$. Then, we can develop an MCMC algorithm to obtain a posterior sample of the copula parameter

$$\mathrm{p}\left(\theta_c\middle|\{u_{(t)}, v_{(t)}\}_{t=1}^{n}\right) \propto \mathrm{p}(\theta_c)\prod_{t=1}^{n} c\left(u_{(t)}, v_{(t)}\middle|\theta_c\right) \qquad (17)$$

Note that the copula parameter(s) can also be estimated using general bivariate dependency measures, such as Kendall's rank correlation and Spearman's rank correlation coefficients.

2.2 Spatial co-occurrence probability using time-varying spatial copulas

To quantify whether global warming is changing the probability of co-occurring warm, dry, and simultaneously warm and dry conditions in different areas of the globe, the present study also introduces a spatial Bayesian, time-varying, conditional multivariate risk framework. The methodology attempts to model time-varying spatial co-occurrence probability of warm and dry conditions between different regions (see Fig. 2 for map of the regions). The advantage of the methodology is that we can model the time-varying dependence structure among multivariate time-varying temperature and precipitation anomalies between each pair region under non-stationary conditions.

First, the weighted averages of annual temperature and precipitation anomalies are calculated for each region. The respective regional time series are then used as the input for the spatial time-varying multivariate risk framework. Details of the spatial dynamic risk framework are given in the following sections.

2.2.1. Spatial co-occurrence probability of warm conditions (or dry conditions)

According to the law of total probability, the posterior predictive probability of the spatial co-occurrence probability of warm years in each pair of regions at time *r* can be formulized as follows

$$\begin{aligned}&\Pr\left(\mathrm{T}_{(\mathrm{i})_{(r)}} > 0, \mathrm{T}_{(\mathrm{i+1})_{(r)}} > 0\middle|\{\mathrm{T}_{(\mathrm{i})_{(t)}}, \mathrm{T}_{(\mathrm{i+1})_{(t)}}\}_{\mathrm{t=1}}^{\mathrm{n}}\right) = \\ &\int \Pr\left(\mathrm{T}_{(\mathrm{i})_{(\mathrm{r})}} > 0, \mathrm{T}_{(\mathrm{i+1})_{(\mathrm{r})}} > 0\middle|\Theta_{\mathrm{c(i,i+1)}}\right)\ \mathrm{p}\left(\Theta_{\mathrm{c(i,i+1)}}\middle|\{\mathrm{T}_{(\mathrm{i})_{(\mathrm{t})}}, \mathrm{T}_{(\mathrm{i+1})_{(\mathrm{t})}}\}_{\mathrm{t=1}}^{\mathrm{n}}\right)\mathrm{d}\,\Theta_{\mathrm{c}}\end{aligned} \qquad (18)$$

where $\boldsymbol{\Theta}_{c(i,i+1)} = \{\{\mu_{\mathrm{T(i)_{(t)}}}, \sigma_{\mathrm{(i)}}\}\{\mu_{\mathrm{T(i+1)_{(t)}}}, \gamma_{\mathrm{(i+1)}}\}, \theta_{\mathrm{c(i,i+1)}}\}$ for each pair of region $(i, i+1)$ is calculated based on the type of the time-varying marginal distributions and also the order of polynomial trend models, expressing the

location parameters through time. For instance, if the time-varying normal and Student's *t* distributions fit to temperature anomaly time series in Region 1, and Region 2, respectively, and a quadratic model describes the trend for the location parameters in both distributions, then the joint parameter set between the regions will be $\boldsymbol{\Theta}_{c(1,2)} = [\eta_{0-2}, \delta_{0-2}, \sigma_{(1)}, \rho_{(2)}, \theta_{c(1,2)}]$. Any combination of the distributions, trend models, and copula functions can be implemented to describe the dependence structure between time-varying co-occurrence probability of warm years for each pair regions. Given $\boldsymbol{\Theta}_{c(i,i+1)}$, we can compute

$$\Pr\left(\mathrm{T}_{(\mathrm{i})_{(r)}} > 0, \mathrm{T}_{(\mathrm{i}+1)_{(r)}} > 0 \middle| \Theta_{\mathrm{c(i,i+1)}}\right) = 1 - F_{\mathrm{T}_{(\mathrm{i})_{(\mathrm{r})}}}\left(0 \middle| \left\{\mu_{\mathrm{T(i)}_{(\mathrm{r})}}, \sigma_{(\mathrm{i})}\right\}\right) - F_{\mathrm{T}_{(\mathrm{i}+1)_{(\mathrm{r})}}}\left(0 \middle| \left\{\mu_{\mathrm{T(i+1)}_{(\mathrm{r})}}, \rho_{(\mathrm{i}+1)}\right\}\right) + C\left(F_{\mathrm{T}_{(\mathrm{i})_{(\mathrm{r})}}}\left(0 \middle| \left\{\mu_{\mathrm{T(i)}_{(\mathrm{r})}}, \sigma_{(\mathrm{i})}\right\}\right), F_{\mathrm{T}_{(\mathrm{i}+1)_{(\mathrm{r})}}}\left(0 \middle| \left\{\mu_{\mathrm{T(i+1)}_{(\mathrm{r})}}, \rho_{(\mathrm{i}+1)}\right\}\right) \middle| \theta_{\mathrm{c(i,i+1)}}\right) \quad (19)$$

The same process is followed to calculate the spatial co-occurrence probability of dry years between each pair of regions. The predictive joint probability of dry years occurring between each pair of regions at time *r* is given by

$$\Pr\left(P_{(i)_{(r)}} < 0, P_{(i+1)_{(r)}} < 0 \middle| \{P_{(i)_{(t)}}, P_{(i+1)_{(t)}}\}_{\mathrm{t=1}}^{\mathrm{n}}\right) = \int \Pr\left(P_{(i)_{(r)}} < 0, P_{(i+1)_{(r)}} < 0 \middle| \Theta_{\mathrm{c(i,i+1)}}\right) \mathrm{p}\left(\Theta_{\mathrm{c(i,i+1)}} \middle| \{P_{(i)_{(t)}}, P_{(i+1)_{(t)}}\}_{\mathrm{t=1}}^{\mathrm{n}}\right) \mathrm{d}\Theta_{\mathrm{c}} \quad (20)$$

where $\boldsymbol{\Theta}_{c(i,i+1)} = \left\{\{\mu_{P(i)_{(t)}}, \gamma_{(i)}\}\{\mu_{P(i+1)_{(t)}}, \kappa_{(i+1)}\}, \theta_{c(i,i+1)}\right\}$ for each pair of region $(i, i+1)$ is calculated based on the time-varying marginal distributions, trends in the mean, and the type of copula functions, accordingly. Given the joint parameter set, then we can calculate

$$\Pr\left(P_{(i)_{(r)}} < 0, P_{(i+1)_{(r)}} < 0 \middle| \Theta_{\mathrm{c(i,i+1)}}\right) = C\left(F_{P_{(i)_{(r)}}}\left(0 \middle| \{\mu_{P(i)_{(r)}}, \gamma_{(i)}\}\right), F_{P_{(i+1)_{(r)}}}\left(0 \middle| \{\mu_{P(i+1)_{(r)}}, \kappa_{(i+1)}\}\right) \middle| \theta_{\mathrm{c(i,i+1)}}\right) \quad (21)$$

It should be noted that the number of combinations to calculate the spatial probability of the extreme conditions between all pairs of regions will be as $n(n-1)/2$, where *n* is the total number of regions. For instance, in this study we have 13 regions, and the spatial co-occurrence probability of the extreme conditions is thus calculated for 78 combinations of the pair regions.

2.2.2. Spatial concurrent probability of warm and dry conditions occurring simultaneously in multiple regions

In this section, we develop a vine copula with time-dependent marginals to calculate time-varying joint probability of years that are both warm and dry occurring simultaneously in each region pair. To model the dependence structure of warm and dry years between each pair region, bivariate copula functions are limited in terms of dimensionality. Therefore, developing a copula with four dimensions would be needed in this case. Alternatively, vine copulas are new tools for constructing complex multi-dimensional dependent models. Vine copulas are graphical models, which decompose multi-dimensional copulas into a hierarchy of paired copulas as building blocks to incorporate more variables in the conditioning sets (*37*). According to Sklar's theorem (*38*), for any *d*-dimensional distribution *F*, with *n* time-varying marginals $x_{1_{(t)}} \dots, x_{d_{(t)}}$, an *d*-dimensional copula, *C*, can be defined as follows

$$F\left(x_{1_{(t)}}, \ldots, x_{d_{(t)}}\right) = C\left(F_1\left(x_{1_{(t)}}\right), \ldots, F_d\left(x_{d_{(t)}}\right)\right) \quad (22)$$

where $F_1\left(x_{1_{(t)}}\right), \ldots, F_d\left(x_{d_{(t)}}\right)$ are time-varying marginal distribution functions. If the time-varying marginals are continuous variables, then the joint density function of a unique multi-dimensional copula is defined as

$$f\left(x_{1_{(t)}}, \ldots, x_{d_{(t)}}\right) = C\left(F_1\left(x_{1_{(t)}}\right), \ldots, F_d\left(x_{d_{(t)}}\right)\right)\prod_{j=1}^{d} f_d\left(x_{d_{(t)}}\right) \quad (23)$$

where *C* is the *d*–dimensional copula density and $f_{1_{(t)}}, \ldots, f_{d_{(t)}}$ are time-varying marginal density functions. Considering a multi-dimensional density as a product of conditional densities, equation (23) can be written as

$$f\left(x_{j_{(t)}}\middle|x_{1:j-1_{(t)}}\right) = c_{j-1,j|1:j-2}\left(F\left(x_{j-1_{(t)}}\middle|x_{j-2_{(t)}}\right), F\left(x_{j_{(t)}}\middle|x_{1:j-2_{(t)}}\right)\right) f\left(x_{j_{(t)}}\middle|x_{1:j-2_{(t)}}\right) \quad (24)$$

where $x_{j-1_{(t)}} = \{x_{1_{(t)}}, \ldots, x_{j-1_{(t)}}\}$. Then the *d*-dimensional density corresponding to the vine copula is given as

$$f\left(x_{1_{(t)}}, \ldots, x_{d_{(t)}}\right) = \prod_{j=1}^{d} f(x_{j_{(t)}}) \prod_{j=2}^{d} \prod_{k=1}^{j-1} c_{j-k,j|1:j-k-1}(F(x_{j-k_{(t)}}|x_{1:j-k-1_{(t)}}), F(x_{j_{(t)}}|x_{1:j-k-1_{(t)}})) \quad (25)$$

where the conditional distribution functions of equation (25) can be driven recursively by the following formula (*39*):

$$F\left(x_{j-k_{(t)}}\middle|x_{1:j-k-1_{(t)}}\right) = \frac{\partial C_{j-k,j-k-1|1:j-k-1}(F\left(x_{j-k_{(t)}}\middle|x_{1:j-k-1_{(t)}}\right), F\left(x_{j-k-1_{(t)}}\middle|x_{1:j-k-1_{(t)}}\right))}{\partial F(x_{j-k-1_{(t)}}|x_{1:j-1_{(t)}})} \quad (26)$$

This derivative is called the *h* function, and has been explicitly solved for the Archimedean and Elliptical copulas. More details are found in *Aas et al.* (*37*).

Depending on the decomposition structure of paired copulas in the graphical structure, two types of regular vine copula families, Canonical vine (C-vine) and D-vine copulas can be defined (*40*). In this study, we use the C-vine copula to calculate the joint probability of warm and dry years occurring simultaneously in each pair region. A C-vine copula is a hierarchical graphical model, which factorizes a *d*-dimensional copula density into the product of $d(d-1)/2$ bivariate conditional copula densities. The specification of decomposing the density for a corresponding four-dimensional C-vine copula (which is the case in this study) can be given as a form of nested set of trees (shown in fig. S2).

The components of a four-dimensional C-vine copula structure with time-varying marginals between each region pair can be factorized and expressed as follows:

$$
\begin{aligned}
&f\left(T_{i_{(t)}}, P_{i_{(t)}}, T_{i+1_{(t)}}, P_{i+1_{(t)}}\right) \\
&= f\left(T_{i_{(t)}}\right).f\left(P_{i_{(t)}}\right).f\left(T_{i+1_{(t)}}\right).f\left(P_{i+1_{(t)}}\right).c_{T_iP_i}\left\{F_{T_{i_{(t)}}}\left(T_{i_{(t)}}\right), F_{P_{i_{(t)}}}\left(P_{i_{(t)}}\right)\right\}\times \\
&\times c_{T_iT_{i+1}}\left\{F_{T_{i_{(t)}}}\left(T_{i_{(t)}}\right), F_{T_{i+1_{(t)}}}\left(T_{i+1_{(t)}}\right)\right\} c_{T_iP_{i+1}}\left\{F_{T_{i_{(t)}}}\left(T_{i_{(t)}}\right), F_{P_{i+1_{(t)}}}\left(P_{i+1_{(t)}}\right)\right\} \\
&\times c_{P_iT_{i+1}|T_i}\left\{F_{P_{i_{(t)}}}\left(P_{i_{(t)}}|\, T_{i_{(t)}}\right), F_{T_{i+1_{(t)}}}\left(T_{i+1_{(t)}}|\, T_{i_{(t)}}\right)\right\} c_{P_iP_{i+1}|T_i}\left\{F_{P_{i_{(t)}}}\left(P_{i_{(t)}}|\, T_{i_{(t)}}\right), F_{P_{i+1_{(t)}}}\left(P_{i+1_{(t)}}|\, T_{i_{(t)}}\right)\right\} \\
&\times c_{T_{i+1}P_{i+1}|T_iP_i}\left\{F_{T_{i+1_{(t)}}}\left(T_{i+1_{(t)}}|\, T_{i_{(t)}}, P_{i_{(t)}}\right), F_{P_{i+1_{(t)}}}\left(P_{i+1_{(t)}}|\, T_{i_{(t)}}, P_{i_{(t)}}\right)\right\} \qquad (27)
\end{aligned}
$$

For the time-varying marginal distributions, two different time-varying normal and Student *t*-distributions are fitted based on the best-selected time-trend models in the time-dependent location parameters as mentioned in section 2.1.1. The posterior distributions of the marginal parameters are then estimated using the Bayesian MCMC method. Different types of the Archimedean and Elliptical copula families – including Gaussian, Student's *t*, Clayton, Gumbel, Frank, and Joe copula functions – are used to fit the decomposed bivariate conditional copula densities in the graphical structure. The Maximum Likelihood Estimation (MLE) method is used to estimate corresponding parameters of the copula functions. The best-fitted copula for each decomposed paired copula function is selected based on the Bayesian Information Criterion (BIC).

Having modeled the C-vine copula with four time-varying dimensions, we next simulate a large sample from the estimated 6-parameter C-vine copula using Monte Carlo simulations. For each simulated value $\left\{u_{i_{(t)}}, v_{i_{(t)}}, u_{i+1_{(t)}}, v_{i+1_{(t)}}\right\}$, the CDF is then inverted to obtain samples for the four dimensions (*i.e.*, temperature and precipitation in each region pair). The corresponding simulation of each dimension is given as follows

$$
\begin{aligned}
T_{i_{(t)}} &= F^{-1}_{T_{i_{(t)}}}\left(u_{i_{(t)}}\middle|\left\{\mu_{\mathrm{T(i)}_{(t)}}, \sigma_{(i)}\right\}\right) \\
P_{i_{(t)}} &= F^{-1}_{P_{i_{(t)}}}\left(v_{i_{(t)}}\middle|\left\{\mu_{P(i)_{(t)}}, \gamma_{(i)}\right\}\right) \\
T_{i+1_{(t)}} &= F^{-1}_{T_{i+1_{(t)}}}\left(u_{i+1_{(t)}}\middle|\left\{\mu_{\mathrm{T(i+1)}_{(t)}}, \sigma_{(i+1)}\right\}\right) \\
P_{i+1_{(t)}} &= F^{-1}_{P_{i+1_{(t)}}}\left(v_{i+1_{(t)}}\middle|\left\{\mu_{P(i+1)_{(t)}}, \gamma_{(i+1)}\right\}\right) \qquad (28)
\end{aligned}
$$

We then evaluate the number of samples that verify the condition $\{T_i > 0, P_i < 0, T_{i+1} > 0, P_{i+1} < 0\}$ between each region pair. Dividing by the total number of simulated samples, we can estimate the time-varying joint probability of warm and dry years occurring simultaneously in each region pair.

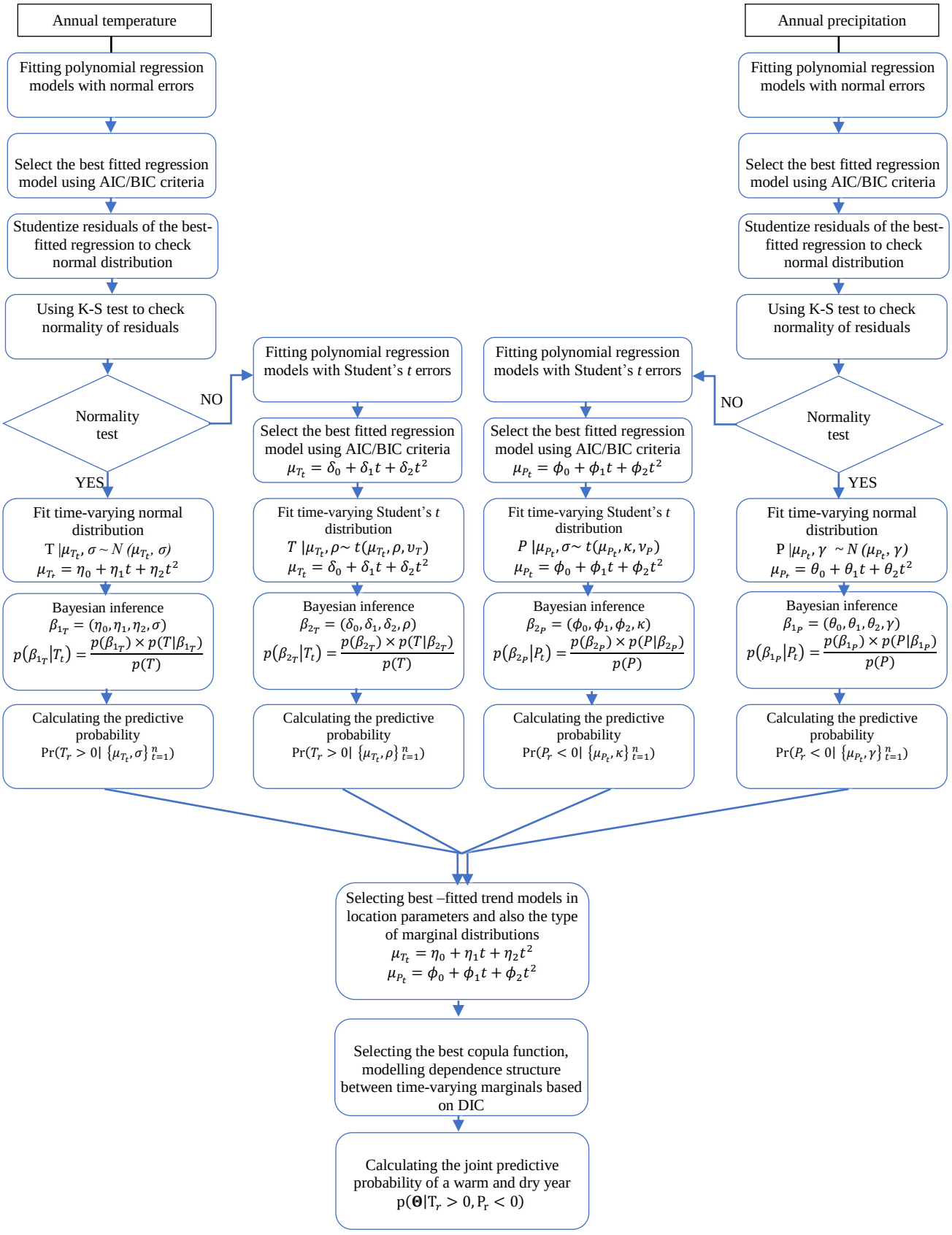

Fig. S1. Schematic flowchart of the methodology to calculate temporal probability of warm, dry, and warm+dry years.

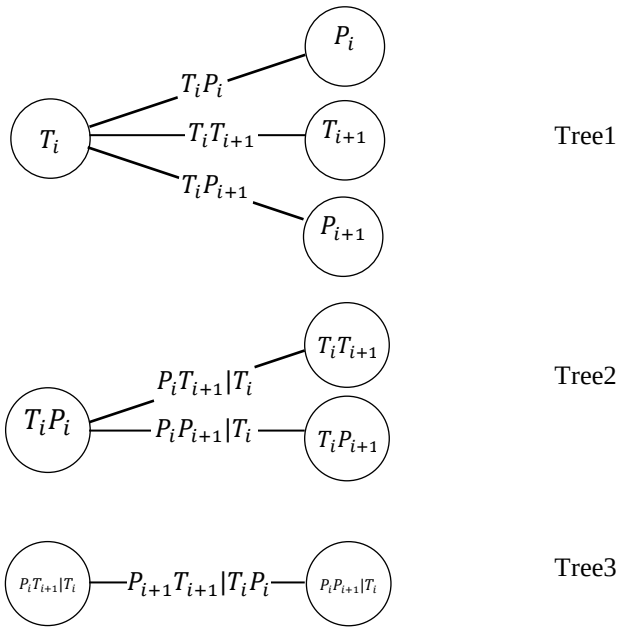

Fig. S2 .A C-vine copula with four dimensions, three trees, and six edges. A C-vine copula with 4 dimensions, 3 trees, and 6 edges. Here, $T_i$and P_i represent temperature and precipitation time series in region i, and T_{i+1} and P_{i+1} represent temperature and precipitation time series in region $i+1$.

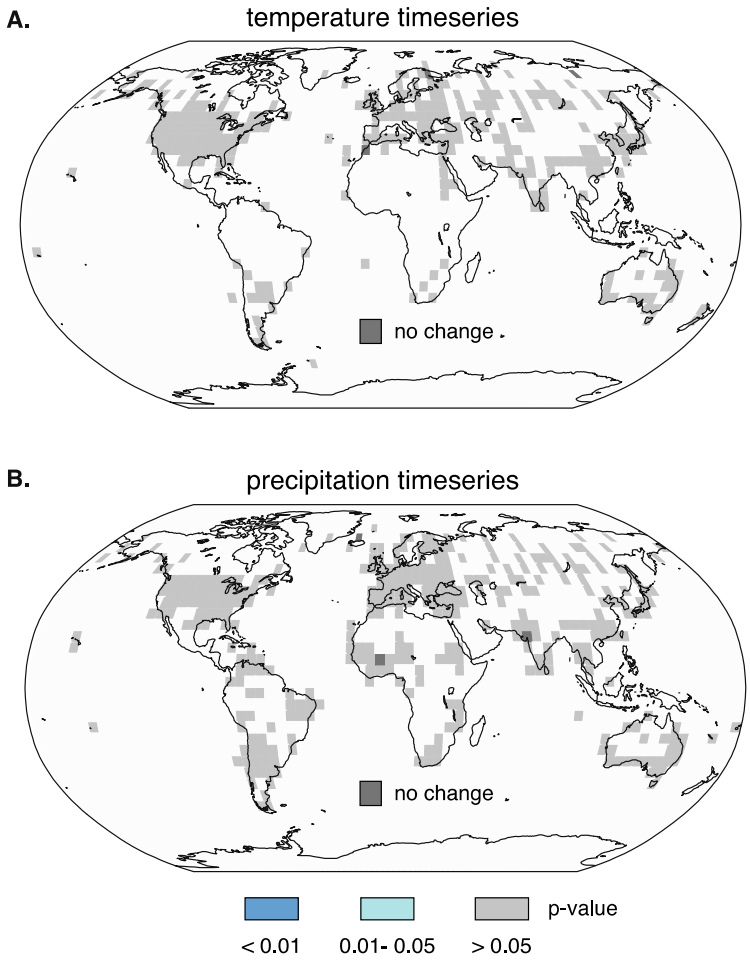

Fig. S3. *P* values for the time trend of the residual time series. P-values are shown from the Block Bootstrapping Mann-Kendall trend analysis on the residuals of the time-trend polynomial regression models applied on the mean of NOAA temperature and precipitation anomaly time series (1931-2015). All grid points have a p-value of >0.05, meaning that there is no grid point in either dataset that exhibits a statistically significant trend in the residuals at the 0.05 level.

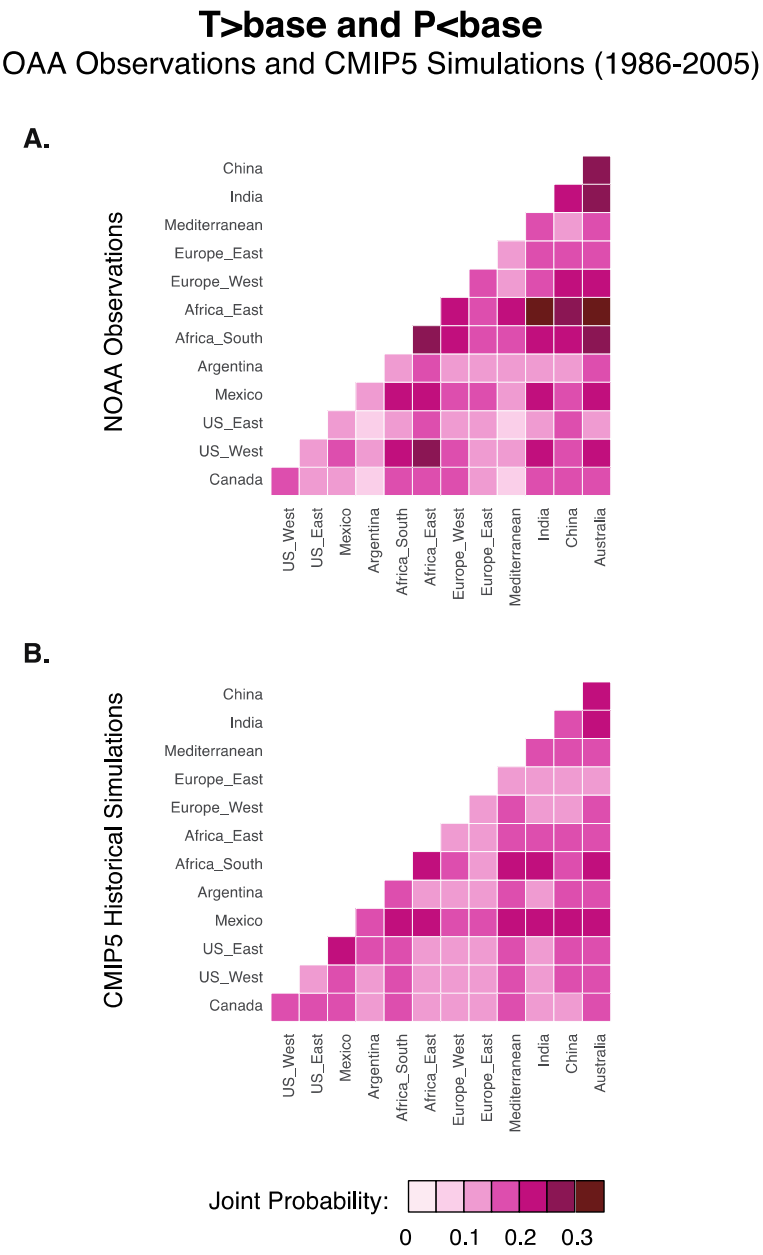

Fig. S4. Comparison of joint probability in the NOAA observations and CMIP5 Historical simulations. Panels show the joint probability of years that are both warm and dry occurring simultaneously in different regions of the world. The top panel shows results from the NOAA Observations. The bottom panel shows the ensemble mean of the results from the CMIP5 Historical climate model realizations. Because the CMIP5 Historical simulations were only run through 2005, we follow the IPCC in using the 1986-2005 period for comparing climate model results with observations.

Table S1. List of climate model realizations for temperature variable used to calculate warm year probability for the CMIP5 Historical and Natural forcing experiments and also for future projections based on RCP2.6 and RCP8.5. Note that for future projections, the realizations are selected based on the availability and also being consistent with the Historical realizations.

	Temperature			
	Historical	Natural	RCP2.6	RCP8.5
1	Bcc-csm1-1_historical_r1i1p1	Bcc-csm1-1_historicalNat_r1i1p1	Bcc-csm1-1_rcp26_r1i1p1	Bcc-csm1-1_rcp85_r1i1p1
2	CanESM2_historical_r2i1p1	BNU-ESM_historicalNat_r1i1p1	CanESM2_rcp26_r2i1p1	CanESM2_rcp85_r2i1p1
3	CanESM2_historical_r4i1p1	CanESM2_historicalNat_r1i1p1	CanESM2_rcp26_r4i1p1	CanESM2_rcp85_r4i1p1
4	CanESM2_historical_r5i1p1	CanESM2_historicalNat_r2i1p1	CanESM2_rcp26_r5i1p1	CanESM2_rcp85_r5i1p1
5	CCSM4_historical_r1i1p1	CanESM2_historicalNat_r4i1p1	CCSM4_rcp26_r1i1p1	CCSM4_rcp85_r1i1p1
6	CCSM4_historical_r2i1p1	CanESM2_historicalNat_r5i1p1	CCSM4_rcp26_r2i1p1	CCSM4_rcp85_r2i1p1
7	CCSM4_historical_r4i1p1	CCSM4_historicalNat_r1i1p1	CCSM4_rcp26_r4i1p1	CCSM4_rcp85_r4i1p1
8	CCSM4_historical_r6i1p1	CCSM4_historicalNat_r2i1p1	CESM1-CAM5_rcp26_r1i1p1	CCSM4_rcp85_r6i1p1
9	CESM1-CAM5_historical_r1i1p1	CCSM4_historicalNat_r4i1p1	CESM1-CAM5_rcp26_r3i1p1	CESM1-CAM5_rcp85_r1i1p1
10	CESM1-CAM5_historical_r3i1p1	CCSM4_historicalNat_r6i1p1	CSIRO-Mk3-6-0_rcp26_r1i1p1	CESM1-CAM5_rcp85_r3i1p1
11	CSIRO-Mk3-6-0_historical_r1i1p1	CESM1-CAM5_historicalNat_r1i1p1	CSIRO-Mk3-6-0_rcp26_r2i1p1	CSIRO-Mk3-6-0_rcp85_r1i1p1
12	CSIRO-Mk3-6-0_historical_r2i1p1	CESM1-CAM5_historicalNat_r3i1p1	CSIRO-Mk3-6-0_rcp26_r3i1p1	CSIRO-Mk3-6-0_rcp85_r2i1p1
13	CSIRO-Mk3-6-0_historical_r3i1p1	CSIRO-Mk3-6-0_historicalNat_r1i1p1	CSIRO-Mk3-6-0_rcp26_r4i1p1	CSIRO-Mk3-6-0_rcp85_r3i1p1
14	CSIRO-Mk3-6-0_historical_r4i1p1	CSIRO-Mk3-6-0_historicalNat_r2i1p1	CSIRO-Mk3-6-0_rcp26_r5i1p1	CSIRO-Mk3-6-0_rcp85_r4i1p1
15	CSIRO-Mk3-6-0_historical_r5i1p1	CSIRO-Mk3-6-0_historicalNat_r3i1p1	GISS-E2-H_rcp26_r1i1p1	CSIRO-Mk3-6-0_rcp85_r5i1p1
16	FGOALS-g2_historical_r1i1p1	CSIRO-Mk3-6-0_historicalNat_r4i1p1	GISS-E2-H_rcp26_r1i1p3	FGOALS-g2_rcp85_r1i1p1
17	FGOALS-g2_historical_r2i1p1	CSIRO-Mk3-6-0_historicalNat_r5i1p1	GISS-E2-R_rcp26_r1i1p1	GISS-E2-H_rcp85_r1i1p1
18	FGOALS-g2_historical_r3i1p1	FGOALS-g2_historicalNat_r1i1p1	GISS-E2-R_rcp26_r1i1p3	GISS-E2-H_rcp85_r2i1p1
19	GISS-E2-H_historical_r1i1p1	FGOALS-g2_historicalNat_r2i1p1	IPSL-CM5A-LR_rcp26_r1i1p1	GISS-E2-R_rcp85_r1i1p1
20	GISS-E2-H_historical_r2i1p1	FGOALS-g2_historicalNat_r3i1p1	IPSL-CM5A-LR_rcp26_r2i1p1	GISS-E2-R_rcp85_r1i1p3
21	GISS-E2-H_historical_r3i1p1	GISS-E2-H_historicalNat_r1i1p1	IPSL-CM5A-LR_rcp26_r3i1p1	GISS-E2-R_rcp85_r2i1p1
22	GISS-E2-H_historical_r5i1p1	GISS-E2-H_historicalNat_r2i1p1	MIROC-ESM-CHEM_rcp26_r1i1p1	IPSL-CM5A-LR_rcp85_r1i1p1
23	GISS-E2-R_historical_r1i1p1	GISS-E2-H_historicalNat_r3i1p1	MIROC-ESM_rcp26_r1i1p1	IPSL-CM5A-LR_rcp85_r2i1p1
24	GISS-E2-R_historical_r1i1p3	GISS-E2-H_historicalNat_r5i1p1	MRI-CGCM3_rcp26_r1i1p1	IPSL-CM5A-LR_rcp85_r3i1p1
25	GISS-E2-R_historical_r2i1p1	GISS-E2-R_historicalNat_r1i1p1		MIROC-ESM-CHEM_rcp85_r1i1p1
26	GISS-E2-R_historical_r2i1p3	GISS-E2-R_historicalNat_r1i1p3		MIROC-ESM_rcp85_r1i1p1
27	GISS-E2-R_historical_r3i1p1	GISS-E2-R_historicalNat_r2i1p1		MRI-CGCM3_rcp85_r1i1p1
28	GISS-E2-R_historical_r3i1p3	GISS-E2-R_historicalNat_r2i1p3		
29	GISS-E2-R_historical_r4i1p1	GISS-E2-R_historicalNat_r3i1p1		
30	GISS-E2-R_historical_r4i1p3	GISS-E2-R_historicalNat_r3i1p3		
31	GISS-E2-R_historical_r5i1p1	GISS-E2-R_historicalNat_r4i1p1		
32	IPSL-CM5A-LR_historical_r1i1p1	GISS-E2-R_historicalNat_r4i1p3		
33	IPSL-CM5A-LR_historical_r2i1p1	GISS-E2-R_historicalNat_r5i1p1		
34	IPSL-CM5A-LR_historical_r3i1p1	IPSL-CM5A-LR_historicalNat_r1i1p1		
35	MIROC-ESM-CHEM_historical_r1i1p1	IPSL-CM5A-LR_historicalNat_r2i1p1		
36	MIROC-ESM_historical_r1i1p1	IPSL-CM5A-LR_historicalNat_r3i1p1		
37	MIROC-ESM_historical_r2i1p1	MIROC-ESM-CHEM_historicalNat_r1i1p1		
38	MRI-CGCM3_historical_r1i1p1	MIROC-ESM_historicalNat_r1i1p1		
39		MIROC-ESM_historicalNat_r2i1p1		
40		MRI-CGCM3_historicalNat_r1i1p1		

Table S2. List of climate model realizations for precipitation variable used to calculate dry year probability for the CMIP5 Historical and Natural forcing experiments and also for future projections based on RCP2.6 and RCP8.5. Note that for future projections, the realizations are selected based on the availability and also being consistent with the Historical realizations

	Precipitation			
	Historical	Natural	RCP2.6	RCP8.5
1	Bcc-csm1-1_historical_r1i1p1	Bcc-csm1-1_historicalNat_r1i1p1	Bcc-csm1-1_rcp26_r1i1p1	Bcc-csm1-1_rcp85_r1i1p1
2	BNU-ESM_historical_r1i1p1	BNU-ESM_historicalNat_r1i1p1	BNU-ESM_rcp26_r1i1p1	BNU-ESM_rcp85_r1i1p1
3	CanESM2_historical_r1i1p1	CanESM2_historicalNat_r1i1p1	CanESM2_rcp26_r1i1p1	CanESM2_rcp85_r1i1p1
4	CanESM2_historical_r2i1p1	CanESM2_historicalNat_r2i1p1	CanESM2_rcp26_r2i1p1	CanESM2_rcp85_r2i1p1
5	CanESM2_historical_r3i1p1	CanESM2_historicalNat_r3i1p1	CanESM2_rcp26_r3i1p1	CanESM2_rcp85_r3i1p1
6	CanESM2_historical_r4i1p1	CanESM2_historicalNat_r4i1p1	CanESM2_rcp26_r4i1p1	CanESM2_rcp85_r4i1p1
7	CanESM2_historical_r5i1p1	CanESM2_historicalNat_r5i1p1	CanESM2_rcp26_r5i1p1	CanESM2_rcp85_r5i1p1
8	CCSM4_historical_r1i1p1	CCSM4_historicalNat_r1i1p1	CCSM4_rcp26_r1i1p1	CCSM4_rcp85_r1i1p1
9	CCSM4_historical_r2i1p1	CCSM4_historicalNat_r2i1p1	CCSM4_rcp26_r2i1p1	CCSM4_rcp85_r2i1p1
10	CCSM4_historical_r4i1p1	CCSM4_historicalNat_r4i1p1	CCSM4_rcp26_r4i1p1	CCSM4_rcp85_r4i1p1
11	CCSM4_historical_r6i1p1	CCSM4_historicalNat_r6i1p1	CESM1-CAM5_rcp26_r1i1p1	CCSM4_rcp85_r6i1p1
12	CESM1-CAM5_historical_r1i1p1	CESM1-CAM5_historicalNat_r1i1p1	CESM1-CAM5_rcp26_r3i1p1	CESM1-CAM5_rcp85_r1i1p1
13	CESM1-CAM5_historical_r3i1p1	CESM1-CAM5_historicalNat_r3i1p1	CSIRO-Mk3-6-0_rcp26_r1i1p1	CESM1-CAM5_rcp85_r3i1p1
14	CSIRO-Mk3-6-0_historical_r1i1p1	CSIRO-Mk3-6-0_historicalNat_r1i1p1	CSIRO-Mk3-6-0_rcp26_r3i1p1	CSIRO-Mk3-6-0_rcp85_r1i1p1
15	CSIRO-Mk3-6-0_historical_r3i1p1	CSIRO-Mk3-6-0_historicalNat_r3i1p1	CSIRO-Mk3-6-0_rcp26_r4i1p1	CSIRO-Mk3-6-0_rcp85_r3i1p1
16	CSIRO-Mk3-6-0_historical_r4i1p1	CSIRO-Mk3-6-0_historicalNat_r4i1p1	CSIRO-Mk3-6-0_rcp26_r5i1p1	CSIRO-Mk3-6-0_rcp85_r4i1p1
17	CSIRO-Mk3-6-0_historical_r5i1p1	CSIRO-Mk3-6-0_historicalNat_r5i1p1	GISS-E2-H_rcp26_r1i1p1	CSIRO-Mk3-6-0_rcp85_r5i1p1
18	FGOALS-g2_historical_r1i1p1	FGOALS-g2_historicalNat_r1i1p1	GISS-E2-R_rcp26_r1i1p1	FGOALS-g2_rcp85_r1i1p1
19	FGOALS-g2_historical_r2i1p1	FGOALS-g2_historicalNat_r2i1p1	GISS-E2-R_rcp26_r1i1p3	GISS-E2-H_rcp85_r1i1p1
20	FGOALS-g2_historical_r3i1p1	FGOALS-g2_historicalNat_r3i1p1	IPSL-CM5A-LR_rcp26_r1i1p1	GISS-E2-H_rcp85_r1i1p3
21	GISS-E2-H_historical_r1i1p1	GISS-E2-H_historicalNat_r1i1p1	IPSL-CM5A-LR_rcp26_r2i1p1	GISS-E2-R_rcp85_r1i1p1
22	GISS-E2-H_historical_r2i1p1	GISS-E2-H_historicalNat_r2i1p1	IPSL-CM5A-LR_rcp26_r3i1p1	GISS-E2-R_rcp85_r1i1p3
23	GISS-E2-H_historical_r3i1p1	GISS-E2-H_historicalNat_r3i1p1	MIROC-ESM-CHEM_rcp26_r1i1p1	GISS-E2-R_rcp85_r2i1p1
24	GISS-E2-H_historical_r5i1p1	GISS-E2-H_historicalNat_r5i1p1	MIROC-ESM_rcp26_r1i1p1	IPSL-CM5A-LR_rcp85_r1i1p1
25	GISS-E2-R_historical_r1i1p1	GISS-E2-R_historicalNat_r1i1p1		IPSL-CM5A-LR_rcp85_r2i1p1
26	GISS-E2-R_historical_r1i1p3	GISS-E2-R_historicalNat_r1i1p3		IPSL-CM5A-LR_rcp85_r3i1p1
27	GISS-E2-R_historical_r2i1p1	GISS-E2-R_historicalNat_r2i1p1		MIROC-ESM-CHEM_rcp85_r1i1p1
28	GISS-E2-R_historical_r2i1p3	GISS-E2-R_historicalNat_r2i1p3		MIROC-ESM_rcp85_r1i1p1
29	GISS-E2-R_historical_r3i1p1	GISS-E2-R_historicalNat_r3i1p1		
30	GISS-E2-R_historical_r3i1p3	GISS-E2-R_historicalNat_r3i1p3		
31	GISS-E2-R_historical_r4i1p1	GISS-E2-R_historicalNat_r4i1p1		
32	GISS-E2-R_historical_r4i1p3	GISS-E2-R_historicalNat_r4i1p3		
33	GISS-E2-R_historical_r5i1p1	GISS-E2-R_historicalNat_r5i1p1		
34	IPSL-CM5A-LR_historical_r1i1p1	IPSL-CM5A-LR_historicalNat_r1i1p1		
35	IPSL-CM5A-LR_historical_r2i1p1	IPSL-CM5A-LR_historicalNat_r2i1p1		
36	IPSL-CM5A-LR_historical_r3i1p1	IPSL-CM5A-LR_historicalNat_r3i1p1		
37	MIROC-ESM-CHEM_historical_r1i1p1	MIROC-ESM-CHEM_historicalNat_r1i1p1		
38	MIROC-ESM_historical_r1i1p1	MIROC-ESM_historicalNat_r1i1p1		
39	MIROC-ESM_historical_r2i1p1	MIROC-ESM_historicalNat_r2i1p1		
40	MIROC-ESM_historical_r3i1p1	MIROC-ESM_historicalNat_r3i1p1		

Table S3. List of climate model realizations available and overlapped for temperature and precipitation variables used to calculate joint warm and dry year probability for the CMIP5 Historical and Natural forcing experiments and also for future projections based on RCP2.6 and RCP8.5. Note that for future projections, the realizations are selected based on the availability and also being consistent with the Historical realizations of both precipitation and temperature variables

	Copula			
	Historical	Natural	RCP2.6	RCP8.5
1	Bcc-csm1-1_historical_r1i1p1	Bcc-csm1-1_historicalNat_r1i1p1	Bcc-csm1-1_rcp26_r1i1p1	Bcc-csm1-1_rcp85_r1i1p1
2	CanESM2_historical_r2i1p1	BNU-ESM_historicalNat_r1i1p1	CanESM2_rcp26_r2i1p1	CanESM2_rcp85_r2i1p1
3	CanESM2_historical_r4i1p1	CanESM2_historicalNat_r1i1p1	CanESM2_rcp26_r4i1p1	CanESM2_rcp85_r4i1p1
4	CanESM2_historical_r5i1p1	CanESM2_historicalNat_r2i1p1	CanESM2_rcp26_r5i1p1	CanESM2_rcp85_r5i1p1
5	CCSM4_historical_r1i1p1	CanESM2_historicalNat_r4i1p1	CCSM4_rcp26_r1i1p1	CCSM4_rcp85_r1i1p1
6	CCSM4_historical_r2i1p1	CanESM2_historicalNat_r5i1p1	CCSM4_rcp26_r2i1p1	CCSM4_rcp85_r2i1p1
7	CCSM4_historical_r4i1p1	CCSM4_historicalNat_r1i1p1	CCSM4_rcp26_r4i1p1	CCSM4_rcp85_r4i1p1
8	CCSM4_historical_r6i1p1	CCSM4_historicalNat_r2i1p1	CESM1-CAM5_rcp26_r1i1p1	CCSM4_rcp85_r6i1p1
9	CESM1-CAM5_historical_r1i1p1	CCSM4_historicalNat_r4i1p1	CESM1-CAM5_rcp26_r3i1p1	CESM1-CAM5_rcp85_r1i1p1
10	CESM1-CAM5_historical_r3i1p1	CCSM4_historicalNat_r6i1p1	CSIRO-Mk3-6-0_rcp26_r1i1p1	CESM1-CAM5_rcp85_r3i1p1
11	CSIRO-Mk3-6-0_historical_r1i1p1	CESM1-CAM5_historicalNat_r1i1p1	CSIRO-Mk3-6-0_rcp26_r3i1p1	CSIRO-Mk3-6-0_rcp85_r1i1p1
12	CSIRO-Mk3-6-0_historical_r3i1p1	CESM1-CAM5_historicalNat_r3i1p1	CSIRO-Mk3-6-0_rcp26_r4i1p1	CSIRO-Mk3-6-0_rcp85_r3i1p1
13	CSIRO-Mk3-6-0_historical_r4i1p1	CSIRO-Mk3-6-0_historicalNat_r1i1p1	CSIRO-Mk3-6-0_rcp26_r5i1p1	CSIRO-Mk3-6-0_rcp85_r4i1p1
14	CSIRO-Mk3-6-0_historical_r5i1p1	CSIRO-Mk3-6-0_historicalNat_r3i1p1	GISS-E2-H_rcp26_r1i1p1	CSIRO-Mk3-6-0_rcp85_r5i1p1
15	FGOALS-g2_historical_r1i1p1	CSIRO-Mk3-6-0_historicalNat_r4i1p1	GISS-E2-R_rcp26_r1i1p1	FGOALS-g2_rcp85_r1i1p1
16	FGOALS-g2_historical_r2i1p1	CSIRO-Mk3-6-0_historicalNat_r5i1p1	GISS-E2-R_rcp26_r1i1p3	GISS-E2-H_rcp85_r1i1p1
17	FGOALS-g2_historical_r3i1p1	FGOALS-g2_historicalNat_r1i1p1	IPSL-CM5A-LR_rcp26_r1i1p1	GISS-E2-R_rcp85_r1i1p1
18	GISS-E2-H_historical_r1i1p1	FGOALS-g2_historicalNat_r2i1p1	IPSL-CM5A-LR_rcp26_r2i1p1	GISS-E2-R_rcp85_r1i1p3
19	GISS-E2-H_historical_r2i1p1	FGOALS-g2_historicalNat_r3i1p1	IPSL-CM5A-LR_rcp26_r3i1p1	GISS-E2-R_rcp85_r2i1p1
20	GISS-E2-H_historical_r3i1p1	GISS-E2-H_historicalNat_r1i1p1	MIROC-ESM-CHEM_rcp26_r1i1p1	IPSL-CM5A-LR_rcp85_r1i1p1
21	GISS-E2-H_historical_r5i1p1	GISS-E2-H_historicalNat_r2i1p1	MIROC-ESM_rcp26_r1i1p1	IPSL-CM5A-LR_rcp85_r2i1p1
22	GISS-E2-R_historical_r1i1p1	GISS-E2-H_historicalNat_r3i1p1		IPSL-CM5A-LR_rcp85_r3i1p1
23	GISS-E2-R_historical_r1i1p3	GISS-E2-H_historicalNat_r5i1p1		MIROC-ESM-CHEM_rcp85_r1i1p1
24	GISS-E2-R_historical_r2i1p1	GISS-E2-R_historicalNat_r1i1p1		MIROC-ESM_rcp85_r1i1p1
25	GISS-E2-R_historical_r2i1p3	GISS-E2-R_historicalNat_r1i1p3		
26	GISS-E2-R_historical_r3i1p1	GISS-E2-R_historicalNat_r2i1p1		
27	GISS-E2-R_historical_r3i1p3	GISS-E2-R_historicalNat_r2i1p3		
28	GISS-E2-R_historical_r4i1p1	GISS-E2-R_historicalNat_r3i1p1		
29	GISS-E2-R_historical_r4i1p3	GISS-E2-R_historicalNat_r3i1p3		
30	GISS-E2-R_historical_r5i1p1	GISS-E2-R_historicalNat_r4i1p1		
31	IPSL-CM5A-LR_historical_r1i1p1	GISS-E2-R_historicalNat_r4i1p3		
32	IPSL-CM5A-LR_historical_r2i1p1	GISS-E2-R_historicalNat_r5i1p1		
33	IPSL-CM5A-LR_historical_r3i1p1	IPSL-CM5A-LR_historicalNat_r1i1p1		
34	MIROC-ESM-CHEM_historical_r1i1p1	IPSL-CM5A-LR_historicalNat_r2i1p1		
35	MIROC-ESM_historical_r1i1p1	IPSL-CM5A-LR_historicalNat_r3i1p1		
36	MIROC-ESM_historical_r2i1p1	MIROC-ESM-CHEM_historicalNat_r1i1p1		
37		MIROC-ESM_historicalNat_r1i1p1		
38		MIROC-ESM_historicalNat_r2i1p1		
39				
40				

Table S4. Elliptical and Archimedean copula functions used in the present study.

Copula	Mathematical function	Parameter range
Gaussian	$\int_{-\infty}^{\phi^{-1}(u_t)} \int_{-\infty}^{\phi^{-1}(v_t)} \frac{1}{2\pi\sqrt{1-\theta^2}} \exp\left(\frac{2\theta xy - x^2 - y^2}{2(1-\theta^2)}\right) dxdy$	$\theta \in [-1,1]$
t	$\int_{-\infty}^{t_{\theta_2}^{-1}(u_t)} \int_{-\infty}^{t_{\theta_2}^{-1}(v_t)} \frac{\Gamma\left(\frac{\theta_2+2}{2}\right)}{\Gamma\left(\frac{\theta_2}{2}\right)\pi\theta_2\sqrt{1-\theta_1^2}} \left(1+\left(\frac{x^2-2\theta_1+xy+y^2}{\theta_2}\right)^{(\theta_2+2)/2} dxdy\right.$	$\theta \in [-1,1]$ and $\theta_2 \in (0,\infty)$
Clayton	$\max\left(u_t^{-\theta} + v_t^{-\theta} - 1, 0\right)^{-1/\theta}$	$\theta \in [-1,\infty]\backslash\{0\}$
Frank	$-\frac{1}{\theta}\ln\left[1+\frac{(\exp(-\theta u_t)-1)(\exp(-\theta v_t)-1)}{\exp(-\theta)-1}\right.$	$\theta \in \mathbb{R}\backslash 0$
Gumbel	$\exp\left\{-\left[(-ln(u_t))^\theta + (-ln(v_t))^\theta\right]^{\frac{1}{\theta}}\right\}$	$\theta \in [1,\infty]$
Joe	$1-[(1-u_t)^\theta + (1-v_t)^\theta - (1-u_t)^\theta(1-v_t)^\theta]^{\frac{1}{\theta}}$	$\theta \in [1,\infty]$